2D CO CRS stack for ocean bottom seismics and multi-component data

T. Boelsen and J. Mann

email: *Tim.Boelsen@gpi.uni-karlsruhe.de*

keywords: *CO CRS stack, ocean bottom seismics, multi-component data, PP and PS imaging*

ABSTRACT

We discuss the application of the 2D Common-Offset (CO) Common-Reflection-Surface (CRS) stack to ocean bottom seismics (OBS) and show a simple synthetic data example including a comparison of model- and data-derived wavefield attributes. Moreover, we present a new approach for the 2D CO CRS stack to process multi-component data and converted waves. By this approach, a distinction between compressional and transversal waves is achieved during the CRS stack. Thus, we can obtain stacked sections and five kinematic wavefield attribute sections separately for PP and PS reflections.

INTRODUCTION

The CRS stack was originally developed to stack (one-component) pre-stack data that were acquired along one straight line into a 2D zero-offset (ZO) section. This technique is referred to as 2D ZO CRS stack, see for instance Mann et al. (1999) and Müller (1999). Zhang et al. (2001) extended the CRS stack in order to stack 2D pre-stack data into a selected finite-offset (FO) gather rather than into a ZO section. If this FO gather is a CO gather this method is referred to as 2D CO CRS stack (Bergler, 2001). In this case the moveout surfaces are described by five kinematic wavefield attributes rather than by three in the ZO case. The search for the wavefield attributes is performed by means of coherence analyses in the pre-stack data volume. Thus, a velocity model of the subsurface is not required to perform the stack except from the near-surface velocities at the sources and receivers in order to calculate wavefield attributes with a geometrical meaning and to compute the search ranges for the attributes.

During the past years, a new marine acquisition geometry was developed which is referred to as ocean bottom seismics (OBS), see Figure 1. By locating the receivers on the sea bottom, it is possible to acquire shear waves in addition to compressional waves and to acquire the seismic data with more than one receiver component. Thus, it is in principal possible to obtain two subsurface images from PP and PS data. A lot of case studies can be found in the literature that show, for instance, an improved image over a leaking gas reservoir zone by generating a PS stack. A second motivation is the potential to get information about S-wave velocities in addition to P-wave velocities. Thus, lithology prediction can be improved.

Bergler (2001) showed that the 2D CO CRS stacking operator can be used to describe traveltimes of PS converted waves by choosing a P-wave velocity at the sources and a S-wave velocity at the receivers. Moreover, Bergler et al. (2002) discussed the application of the 2D CO CRS stack to data that were acquired with two components (vertical and horizontal). However, in this approach the CRS stack was performed with both components separately and the distinction between both wave types was achieved after the CRS stack.

The objective of this paper is to show that the 2D CO CRS stack is able to handle the OBS acquisition geometry and to present a technique that yields the distinction between PP and PS reflections during the CRS stack to obtain a PP and a PS CO CRS stacked section and five kinematic wavefield attribute sections for each of the both wave types.

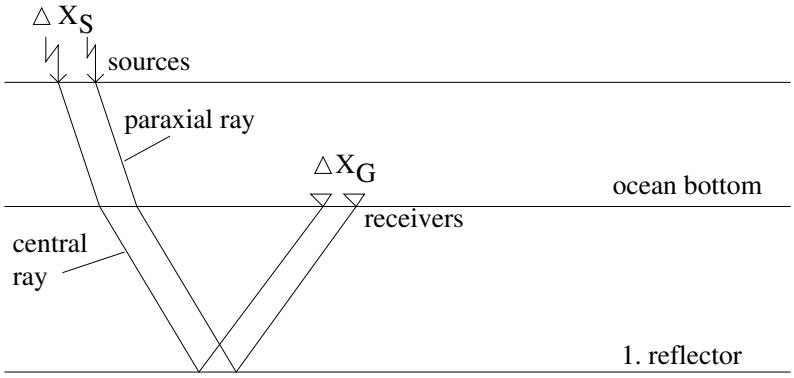

Figure 1: An arbitrarily chosen central ray and a paraxial ray in the close vicinity of the central ray for the OBS acquisition geometry.

CO CRS STACKING OPERATOR FOR OBS GEOMETRIES

Let us consider Figure 1 that shows a simple sketch of an 2D OBS acquisition geometry with the receivers located on the sea bottom and the sources (e.g. airguns) placed some meters below the water surface. We assume the sea bottom to be horizontal without any topography and that all sources are disposed in the same water depth. The figure shows an arbitrarily chosen central ray that starts at a source and ends at a receiver after being reflected at the shown interface below the ocean bottom. In addition, a paraxial ray in the close vicinity of the central ray is depicted. The horizontal displacement between the sources of both rays is called Δx_S and between the receivers Δx_G. From the figure we observe that

$$\Delta z_S \equiv 0 \quad \text{and} \quad \Delta z_G \equiv 0 \quad , \tag{1}$$

where Δz_S and Δz_G are the vertical displacements between the sources and receivers, respectively. This means that we may use the so-called conventional 2D CO CRS stacking operator that was originally developed to stack data that were acquired along one straight line. This operator can be written as (Bergler (2001) and Zhang et al. (2001))

$$\begin{aligned} T^2(\Delta x_S, \Delta x_G) = & \left[t_0 + \frac{\sin\beta_G}{v_G}\,\Delta x_G - \frac{\sin\beta_S}{v_S}\,\Delta x_S \right]^2 \\ & + 2\,t_0 \left[\Delta x_S\,(K_1 - K_3)\,\frac{\cos^2\beta_G}{v_G}\,\Delta x_G \right. \\ & + \frac{1}{2}\,\Delta x_S \left((K_1 - K_3)\,\frac{\cos^2\beta_G}{v_G} - K_2\,\frac{\cos^2\beta_S}{v_S} \right) \Delta x_S \\ & \left. + \frac{1}{2}\,\Delta x_G\,K_1\,\frac{\cos^2\beta_G}{v_G}\,\Delta x_G \right] \end{aligned} \tag{2}$$

in source and receiver dislocation coordinates Δx_S and Δx_G and as

$$\begin{aligned} T^2(\Delta x_m, \Delta h) = & \left[t_0 + \left(\frac{\sin\beta_G}{v_G} - \frac{\sin\beta_S}{v_S} \right) \Delta x_m + \left(\frac{\sin\beta_G}{v_G} + \frac{\sin\beta_S}{v_S} \right) \Delta h \right]^2 \\ & + t_0 \left[\Delta x_m\,2 \left(K_3\,\frac{\cos^2\beta_G}{v_G} + K_2\,\frac{\cos^2\beta_S}{v_S} \right) \Delta h \right. \\ & + \Delta x_m \left((4\,K_1 - 3\,K_3)\,\frac{\cos^2\beta_G}{v_G} - K_2\,\frac{\cos^2\beta_S}{v_S} \right) \Delta x_m \\ & \left. + \Delta h \left(K_3\,\frac{\cos^2\beta_G}{v_G} - K_2\,\frac{\cos^2\beta_S}{v_S} \right) \Delta h \right] \end{aligned} \tag{3}$$

in midpoint and half-offset coordinates. Equations (2) and (3) show the hyperbolic traveltime formulas in terms of wavefront curvatures K_1, K_2, and K_3 of waves propagating along the central ray: K_1 is defined

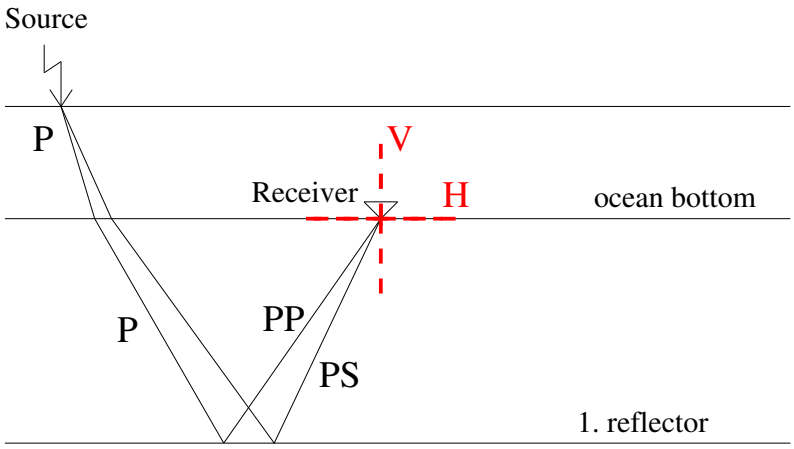

Figure 2: Multi-component data acquisition with vertical and horizontal components in the OBS case. Only primary PP and PS reflections are considered.

as the wavefront curvature of an emerging wave at the receiver in a common-shot (CS) experiment while K_2 and K_3 are the wavefront curvatures in a (hypothetical) common-midpoint (CMP) experiment at the source and receiver, respectively, see Bergler (2001). Please note that Zhang et al. (2001) use a different notation for the wavefront curvatures. t_0 is the two-way traveltime along the central ray and β_S and β_G are the emergence angles of the central ray at the source and receiver, respectively. v_S and v_G are the near-surface velocities in the vicinities of the source and the receiver, respectively.
As long as we assume that both surfaces on which the sources and receivers are located are flat (no topography at the sea bottom and all sources disposed in the same water depth), the CO CRS stack is able to handle OBS acquisition geometries.

In contrast, the conventional ZO CRS stacking operator is not able to handle the OBS acquisition geometry since the downgoing and upgoing raypaths are not identical, i. e., the simulated ZO rays would, in general, not be normal rays and the first spatial derivatives with respect to half-offset would not vanish. Thus, a description by means of three wavefield attributes is not possible and the more general traveltime formulas (see Equations (2) or (3)) depending on five wavefield attributes have to be taken.

If there is surface topography present at the ocean bottom it is possible to use a traveltime formula that takes the topography into account or to use the conventional traveltime formula with a correction of the wavefield attributes afterwards. For more details, we refer to Boelsen (2004) in this report.

PROCESSING OF MULTI-COMPONENT DATA

In the following, we want to present a new approach for the 2D CO CRS stack that is able to separate PP and PS reflections during the CRS stack. Let us consider Figure 2 that again shows a simple sketch of an OBS acquisition geometry with the receivers located on the seafloor. Now we assume that the data are acquired with two components, namely with global vertical and horizontal components in the plane defined by the two source and receiver lines. We refer to the vertical and horizontal components as V and H, respectively. We consider two different types of waves, namely PP and PS waves. The former ones do not convert into S-waves while propagating through the medium from the source to the receiver. The latter ones start at the source as P-waves and reach the receiver as S-waves, i. e., conversion into S-waves occurs somewhere in the subsurface. In general, both wave types are present on both components and the task is to distinguish between both types in order to perform a PP and a PS CO CRS stack.

General idea

The key information for this method is the emergence angle β_G at the receivers which is an additional output of the CO CRS stack. This angle describes the ray direction of an emerging wave. During the CRS stack, $\sin\beta_G/v_G$ is determined. Depending on the chosen near-surface velocity, P- or S-wave velocity, we

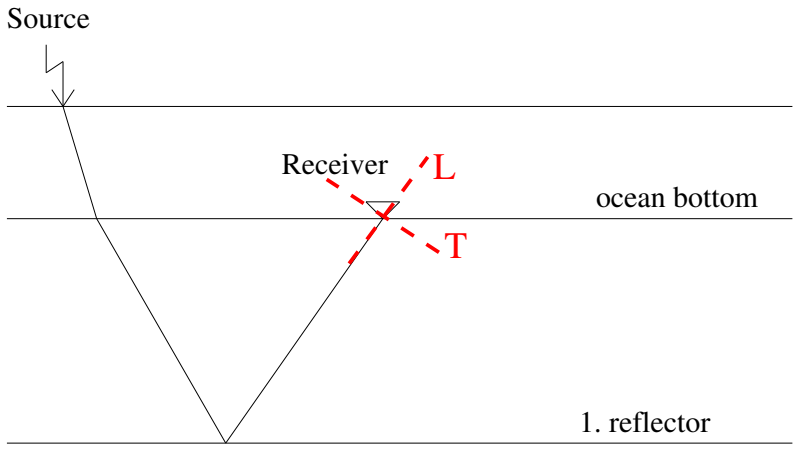

Figure 3: After the rotation of the vertical and horizontal components into the ray-centered coordinate system we obtain the longitudinal and transversal components.

can calculate the emergence angles for emerging P- or S-waves, respectively.
After the determination of the emergence angle β_G we can rotate the global coordinate system defined by the vertical and horizontal components V and H by β_G:

$$\begin{pmatrix} T \\ L \end{pmatrix} = \begin{pmatrix} \cos\beta_G & \sin\beta_G \\ -\sin\beta_G & \cos\beta_G \end{pmatrix} \begin{pmatrix} H \\ V \end{pmatrix} . \tag{4}$$

In Equation (4) L and T denotes the longitudinal and transversal components, respectively, in a ray-centered coordinate system. The situation after the rotation is depicted in Figure 3. Solving Equation (4) with respect to T and L yields

$$T = \cos\beta_G\, H + \sin\beta_G\, V \quad \text{and} \quad L = -\sin\beta_G\, H + \cos\beta_G\, V\,. \tag{5}$$

We assume an isotropic medium and, moreover, we neglect any surface effects at the sea bottom (e.g. transmission). Choosing the near-surface velocity v_G to be the P-wave velocity, $v_G = v_G^P$, the direction of the ray at the receiver given by β_G defines the polarization direction of an emerging P-wave (tangential to the ray) traveling along this ray. Thus, the longitudinal component L given by Equation (5) contains this PP reflection. In a second step, the S-wave velocity is used as the near-surface velocity at the receiver. In that case the expected polarization direction of an emerging S-wave traveling along that ray would then be normal to the ray direction, defined by β_G, with the assumptions made above. Thus, the transversal component T given by Equation (5) can be used to get this PS event.

Implementation

Implementing the above-described idea to separate PP and PS reflections we have to take into account that the emergence angles of paraxial rays are, in general, different from the emergence angle of the central ray. Let us denote the emergence angle of the central ray by β_G. The emergence angle of any paraxial ray, γ, can then be approximated by (modified after Höcht et al., 1999)

$$\sin\gamma = \mathrm{sgn}(R_G)\,\frac{R_G\sin\beta_G + \Delta x_G}{\sqrt{R_G^2 + 2R_G\Delta x_G\sin\beta_G + \Delta x_G^2}}\,, \tag{6}$$

where $R_G = 1/K_G$ is the radius of curvature of the emerging wavefront traveling along the central ray at the receiver and Δx_G the horizontal displacement between the receiver of the central ray and the receiver of the considered paraxial ray. The only assumption made in Equation (6) is that the emerging wavefront has locally a circular shape. Please note that Equation (6) is not valid for a common-receiver (CR) configuration. In this case we have $R_G = 0$ and $\Delta x_G = 0$ and, thus, a singularity in Equation (6). However, this singularity is removable. An alternative parametrization can be found in Höcht et al. (1999).

The conventional CO CRS stacking procedure to stack one-component data considering only one wave type (see Bergler (2001)) has to be modified in order to separate PP and PS reflections from two components.

For the method introduced here we propose the following search strategy:

1. A first search in the CS gathers.
2. A second search in the CS stacked CO gathers.
3. A final search in the CMP gathers.
4. Using the determined wavefield attributes, the final CO CRS stack can be performed as a last step.

In the following we will explain these four steps in detail. In each above mentioned subset of the multicoverage data volume (CS, CO, and CMP gather) the stacking operator given by Equation (2) or (3) simplifies and reduces to a curve rather than a surface. For each gather the operator has the same structure of an equation with one variable, namely

$$T^2(y) = (t_0 + ay)^2 + by^2, \tag{7}$$

where a and b are the dip and the curvature of the traveltime curve, respectively. The variable y depends on the considered subset of the data.

Step I: CS search In a CS gather the variable y reads Δx_G. From Equation (2) we see that a and b are given in a CS gather by

$$a_{\text{CS}} = \frac{\sin\beta_G}{v_G}, \quad b_{\text{CS}} = t_0 \left(K_1 \frac{\cos^2\beta_G}{v_G} \right). \tag{8}$$

Thus, the emergence angle β_G is directly available from the dip and the wavefront curvature $K_G = K_1$ of the emerging wave at the receiver can directly be calculated from the traveltime curvature. This is required to find the emergence angles of the paraxial rays γ, see Equation (6). This implies that a two-parameter search for the attributes has to be performed, i. e., we have to search for the dip and curvature simultaneously. Knowing the emergence angles of the central ray and the paraxial rays in the aperture, we can perform the rotation of the vertical and horizontal components by these angles to get the longitudinal and transversal ones. In a first step we choose the near-surface velocity at the receiver in Equation (8) to be the P-wave velocity. Thus, we calculate the emergence angle and the wavefront curvature of a P-wave and we have to take the longitudinal components for the coherence analysis and the CS stack after having found the dip and curvature with the highest coherence value. In a second step the S-wave velocity is chosen as the near-surface velocity at the receiver to get the emergence angle and wavefront curvature of an emerging S-wave. After the rotation, we now use the transversal components for the coherence analyses and final CS stack. In that way we are able to distinguish between PP and PS reflections and obtain a PP CS stacked CO section and a PS CS stacked CO section.

Step II: CO search This step is much easier and faster than the first one. Since the search is performed in the two CO gathers obtained by the CS stack in the first step, we do not have to distinguish between the different wave types and can run two independent search routines in the two CO gathers. a and b are given in a CO gather by (see Equation (3))

$$a_{\text{CO}} = \frac{\sin\beta_G}{v_G} - \frac{\sin\beta_S}{v_S}, \quad b_{\text{CO}} = t_0 \left((4\,K_1 - 3\,K_3)\frac{\cos^2\beta_G}{v_G} - K_2\frac{\cos^2\beta_S}{v_S} \right), \tag{9}$$

while y is Δx_m. In principle, this CO search is analog to the one implemented in the conventional CO CRS stack and can be performed as a two-parameter search or two one-parameter searches. As an output this yields two CO stacked CO sections, one for PP and one for PS reflections.

Step III: CMP search So far we have determined four kinematic wavefield attributes, namely a_{CS}, b_{CS}, a_{CO}, and b_{CO}. To search for the fifth attribute (a third curvature) we have to use the two-component pre-stack data again. We propose to perform the search in CMP gathers. Please note that we cannot use the common-receiver (CR) gathers since we need the emergence angles and wavefront curvatures at the receivers to distinguish between the two considered wave types. In a CMP gather y reads Δh while the dip and curvature of the traveltime is given by (see Equation (3))

$$a_{\mathrm{CMP}} = \frac{\sin\beta_G}{v_G} + \frac{\sin\beta_S}{v_S}\,, \quad b_{\mathrm{CMP}} = t_0\left(K_3\frac{\cos^2\beta_G}{v_G} - K_2\frac{\cos^2\beta_S}{v_S}\right)\,. \tag{10}$$

A one-parameter search for b_{CMP} is sufficient since we can calculate a_{CMP} by means of a_{CS} and a_{CO} (see Equations (8) and (9)). For each tested value of b_{CMP} during the CMP search we can calculate the wavefront curvature K_3 or the radius of curvature $R_3 = 1/K_3$ at the receiver by means of b_{CMP} and the results from the first two searches (see again Equations (8) and (9)). We need this information in order to get the emergence angles of the paraxial rays that contribute to the coherence analyses and CMP stack, see Equation (6). β_G is already known from the CS search. Finally, the same procedure as during the CS stack can be performed to distinguish between PP and PS reflections, i. e., choice of the near-surface velocity for P- or S-waves, rotation of the vertical and horizontal components and consideration of the longitudinal or transversal components, respectively, for coherence analyses to find the optimum value of b_{CMP} for which the calculated traveltime curve fits best the reflection events in the data. The result of this step are a PP and a PS CMP stacked CO section.

Step IV: CO CRS stack Now we have determined all five wavefield attributes that we need to perform the CO CRS stack. In fact we have ten attributes, five for PP and five for PS reflections. Again, the emergence angles of the paraxial rays that contribute to the CRS stack are required in order to achieve the distinction between PP and PS reflections. Thus, the main task is to find the wavefront curvature K_G at the considered receiver which depends on the measurement configuration. The emergence angle β_G of the considered central ray is already known and does not depend on the measurement configuration. To determine K_G we consider an arbitrary measurement configuration which is described by

$$\Delta x_G = l\,\Delta x_S\,, \tag{11}$$

where Δx_G and Δx_S are the horizontal displacements between the receivers and sources, respectively, of the central and a paraxial ray and l is a real number. Let us consider Figure 4. $\overline{x}_S$ and $\overline{x}_G$ are the shot and receiver positions, respectively, of a paraxial ray while x_S and x_G are the corresponding positions of the central ray. For the CS configuration, for instance, we have $l = \infty$ and, thus, $K_G = K_1$ and for the CR configuration we have $l = 0$ and $K_G = \infty$. Bergler (2001) derived an equation to calculate K_G if K_1, K_3, and l are known:

$$K_G = K_1\left(1 + \frac{1}{l}\right) - \frac{K_3}{l}\,. \tag{12}$$

To summarize, the last step is performed as follows: Since five wavefield attributes are available for each time sample of the CO section to be simulated we can calculate the CO CRS stacking surface given by, for instance, Equation (3). The choice of the near-surface velocity v_G depends on the wave type we want to consider. For each paraxial ray within the stacking aperture we have to determine the parameter l in order to calculate the wavefront curvature K_G at the receiver of the considered central ray by using Equation (12). K_1 and K_3 are determined for each time sample. Since we know the emergence angle β_G of the central ray it is possible to calculate the emergence angle γ of any arbitrary paraxial ray by means of Equation (6) and K_G. In a next step the rotation by γ is performed which yields the longitudinal and transversal component. For a PP reflection we use the amplitude of the longitudinal component and for a PS reflection we have to use the amplitude of the transversal component. Doing this for each paraxial ray within the stacking aperture we can sum up the amplitudes along the stacking surface and assign the stacking result to the respective CO time sample. In that way, we obtain two CO CRS stack sections, for PP and PS reflections. To see how well the stacking surfaces fit to events in the pre-stack data volumes it is possible to compute the coherence values for each time sample.

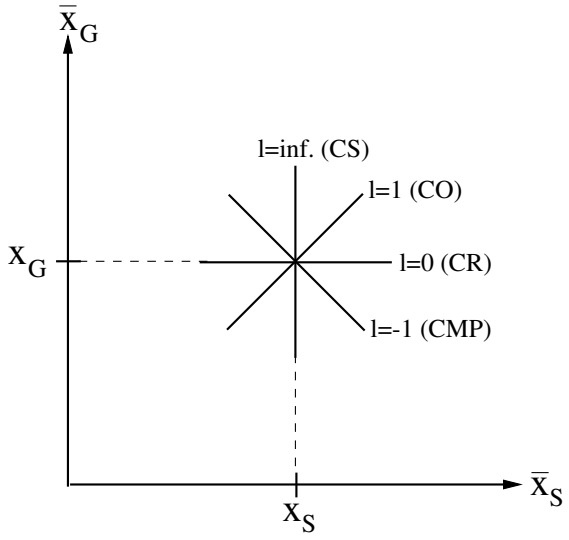

Figure 4: The common-shot (CS), common-offset (CO), common-receiver (CR), and common-midpoint (CMP) measurement configuration defined by l in the $(\overline{x}_S - \overline{x}_G)$-plane.

We want to stress that in order to apply this strategy to seismic data, a reasonable number of traces in CS gathers within the stacking aperture is required. In practice, this means that the distance between the receivers should not be too large and that a sufficient number of receivers is used. Otherwise, an accurate and stable determination of dips and curvatures of traveltime curves and, therewith, of emergence angles and wavefront curvatures particularly during the CS search is not possible. Specifically, for OBS acquisition geometries this means that data acquired with receiver cables (with multi-component geophones) located on the sea bottom are more suitable than data acquired with single geophones since in the latter case the distance between the geophones is, in general, much larger and the number of geophones is low so that there are not enough traces in a CS gather within a reasonable stacking aperture.

SYNTHETIC DATA EXAMPLE

In order to show the application of the stacking operator given by Equation (2) or (3) to OBS data, we created a simple synthetic data set. We considered only primary PP reflections that were acquired with the pressure component to show the validity of the stacking operator to the OBS acquisition geometry. For this purpose we will compare the model- and data-derived wavefield attributes.

The model used to generate the synthetic data is shown in Figure 5. It consists of five homogeneous layers separated by four curved as well as non-curved interfaces. The uppermost layer is the water layer, the sources are located in a water depth of six meters. The receivers are placed along the first interface (counted from the surface) which represents a horizontal sea bottom. Also depicted in Figure 5 are seismic rays from a CS experiment that are reflected at the second interface below the sea bottom.

For this model, a multi-coverage data set was generated. Primary PP reflections were simulated for the three interfaces below the sea bottom by a ray tracer for half-offsets from $h = 0\,\text{km}$ to $h = 2\,\text{km}$ in increments of $\Delta h = 0.025\,\text{km}$ and midpoint intervals of $\Delta x_m = 0.025\,\text{km}$ in the range $2\,\text{km} \leq x_m \leq 7\,\text{km}$. As a seismic signal, we used a zero-phase Ricker wavelet of 30 Hz peak frequency. The sampling interval was 4 ms. Finally, random noise was added to the data set so that all CO sections look with respect to their signal-to-noise ratio similar to the one for half-offset $h = 0.5\,\text{km}$ (see Figure 6). This particular CO section has been simulated by the CO CRS stack.

Figure 6 also shows the CO section obtained by the CO CRS stack. The signal-to-noise ratio is dramatically increased and all three reflectors are clearly visible. In addition to the high-quality stacked section, we obtain five wavefield attribute sections for β_S, β_G, K_1, K_2, and K_3 if the near-surface velocities at the receivers and sources, v_G and v_S, respectively, are known. These attributes can be used for further analyses, like the determination of the geometrical spreading factor (see Zhang et al. (2001)). The five attribute

sections as well as the coherence section associated with the CO CRS stack are depicted in Figures 7 and 8.

As long as the reflection events can be approximated by hyperbolae within a certain aperture, it is expected that the CRS stack works properly since then it is possible to find stacking surfaces that fit well the events if the search ranges are chosen correctly. An important point is whether the determined kinematic wavefield attributes have the correct geometrical meaning. In order to check how accurate the CO CRS stack determined the attributes, we compared the found, so-called data-derived, attributes with the exact model-derived ones. The model-derived attributes could be obtained by means of a ray tracer while the data-derived attributes were extracted from the different attribute sections along the three traveltime curves that are associated with the primary PP reflections from each interface of the model. The corresponding traveltimes could be obtained with the ray tracer, too.

Figures 9(a) and 9(b) show the model- and data-derived emergence angles β_S and β_G, respectively, for the PP reflections from all three interfaces. The very good coincidence between the exact attributes (solid) and the attributes determined by the CO CRS stack (dotted) is clearly visible. For all samples, the deviation is lower than half a degree.
Figures 9(c)-9(e) show the comparison of the model- and data-derived wavefront curvatures K_1, K_2, and K_3, respectively. The data-derived curvatures (dotted) show some fluctuations around the model-derived values (solid) but they are still in good agreement with them. The largest deviations occur around CMP no. 60 for the second reflector and around CMP no. 100 for the third reflector. By considering Figure 7, we observe that these deviations coincide very well with low coherence values. Moreover, K_2 and K_3 are not very accurately determined where rapid curvature changes occur, for instance in the presence of caustics.

Please note that the accuracy of the determined wavefield attributes depends on the chosen aperture for the search routines. The best possible aperture that yields the most accurate wavefield attributes has to be found out empirically. If the wavefield attributes are used for further analyses, we propose to optimize and smooth the attributes. This could also improve the stacking results. The attributes that were found by the initial stack would then be used as input values for the optimization. In this example, the initial attributes are very close to the exact ones and it can be expected that the optimization would yield even more accurate attributes. Both steps, optimization and event-consistent smoothing of wavefield attributes, have already been developed for the ZO CRS stack and are currently under investigation for the CO CRS stack.

CONCLUSIONS

We have discussed that the conventional CO CRS stacking operator can handle OBS acquisition geometries as long as there are no significant vertical displacements between the sources or between the receivers, i. e., as long as there is no topography present at the sea bottom and the sources are placed in the same water depth. The application to synthetic data yielded a high-quality stacked section with a dramatically increased signal-to-noise ratio and five kinematic wavefield attribute sections that can be used for further analyses. A comparison of the determined wavefield attributes with the exact model-derived ones showed that the CO CRS stack provided accurate emergence angles and good results for the wavefront curvatures, too. To further improve the results, optimization and event-consistent smoothing steps should be applied.
Moreover, we have presented a new approach in order to stack two-component data by means of the 2D CO CRS stack. This approach is able to distinguish between PP and PS reflections by combining operator shape and orientation with polarization information and provides stacked sections and kinematic wavefield attribute sections for both wave types. An application of this method to synthetic data is currently investigated. Further tests with real data, for instance with multi-component OBS or vertical seismic profile (VSP) data, are required. A stacking operator for a VSP acquisition geometry is given in Boelsen (2004) in this report.

ACKNOWLEDGMENTS

This work was kindly supported by the sponsors of the *Wave Inversion Technology (WIT) Consortium*, Karlsruhe, Germany.

REFERENCES

Bergler, S. (2001). The Common-Reflection-Surface Stack for Common Offset – Theory and Application. Master's thesis, University of Karlsruhe.

Bergler, S., Duveneck, E., Höcht, G., Zhang, Y., and Hubral, P. (2002). Common-Reflection-Surface Stack for converted waves. *Studia Geophysica et Geodaetica*, 46:165–175.

Höcht, G., de Bazelaire, E., Majer, P., and Hubral, P. (1999). Seismics and optics: hyperbolae and curvatures. *Journal of Applied Geophysics*, 42(3,4):261–281.

Mann, J., Jäger, R., Müller, T., Höcht, G., and Hubral, P. (1999). Common-reflection-surface stack - a real data example. *Journal of Applied Geophysics*, 42(3,4):301–318.

Müller, T. (1999). *The Common Reflection Surface Stack Method - Seismic imaging without explicit knowledge of the velocity model*. PhD thesis, University of Karlsruhe.

Zhang, Y., Bergler, S., and Hubral, P. (2001). Common-Reflection-Surface (CRS) stack for common-offset. *Geophysical Prospecting*, 49:709–718.

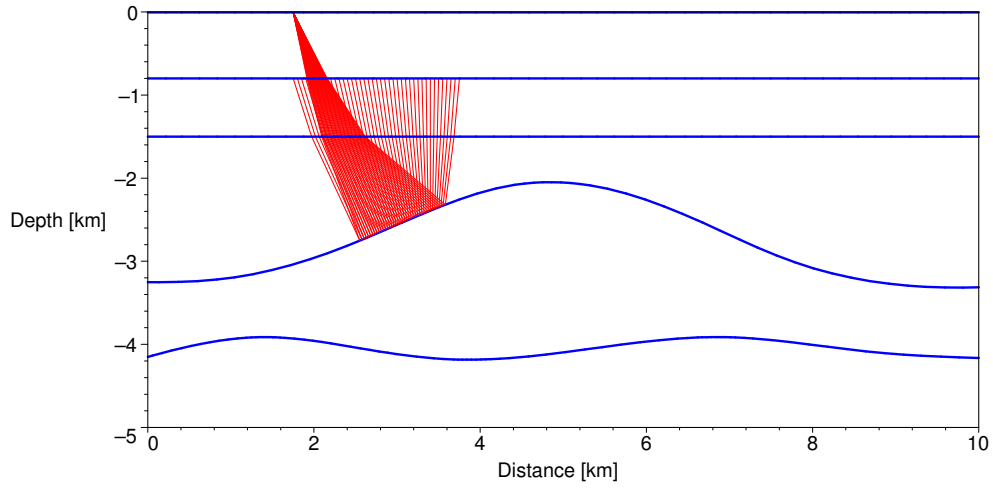

Figure 5: Model used to generate the synthetic data. To illustrate the OBS acquisition geometry, we depicted seismic rays that are reflected at the dome-like interface from one CS experiment.

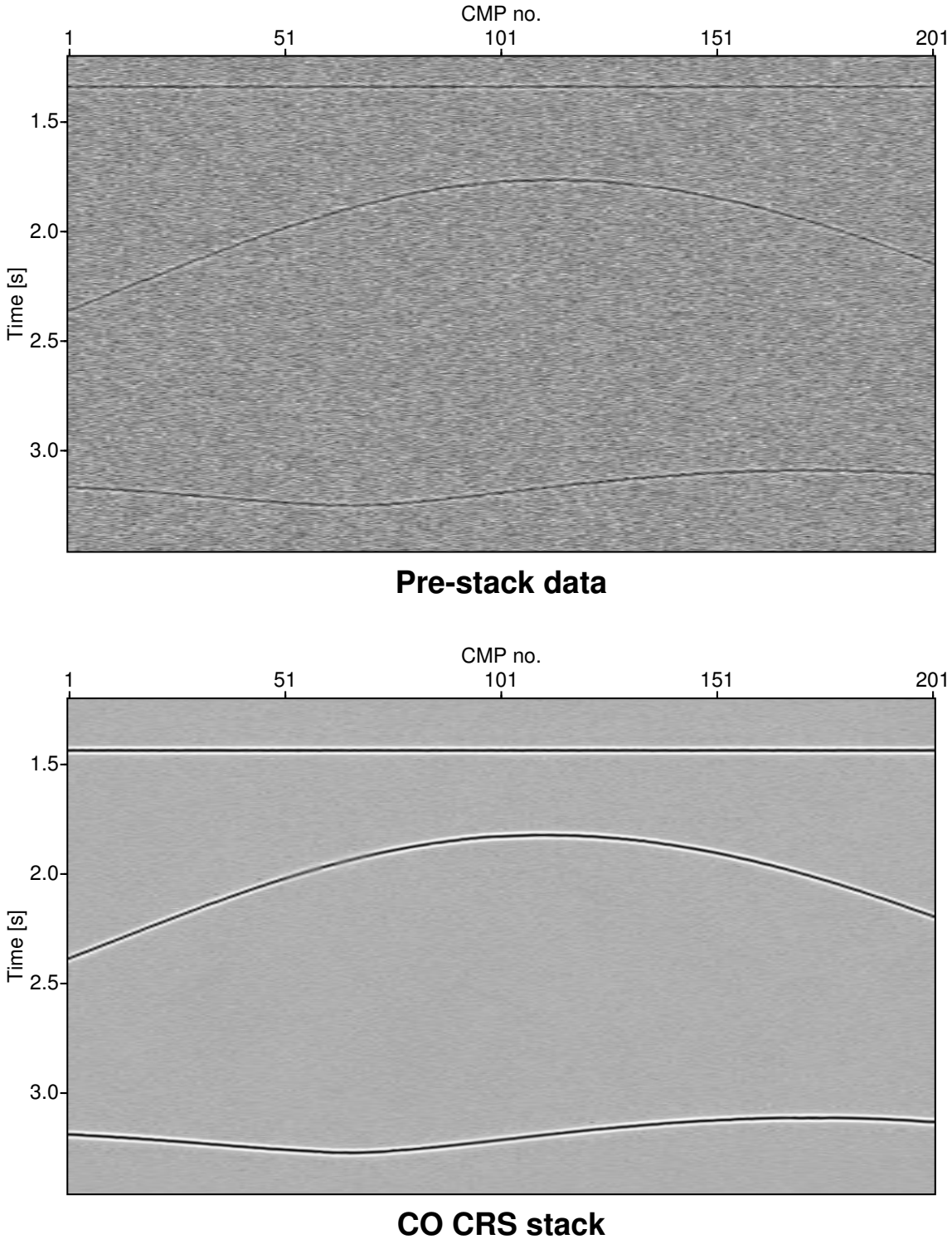

Figure 6: Pre-stack CO section ($h = 500\,\mathrm{m}$) for the model shown in Figure 5 and the same CO section after the CO CRS stack.

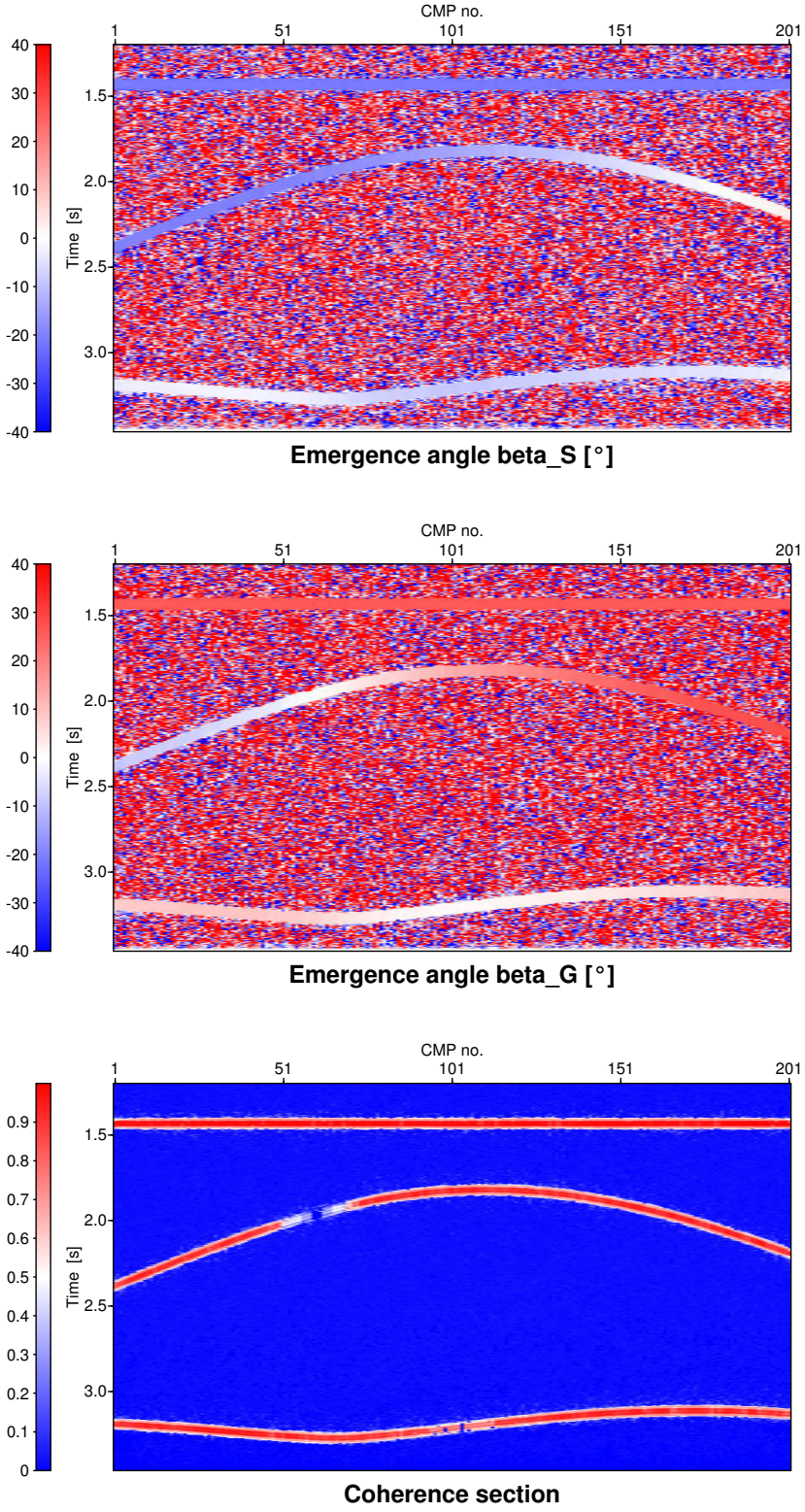

Figure 7: Emergence angles β_S and β_G determined by the CO CRS stack as well as the coherence section associated with the CO CRS stack.

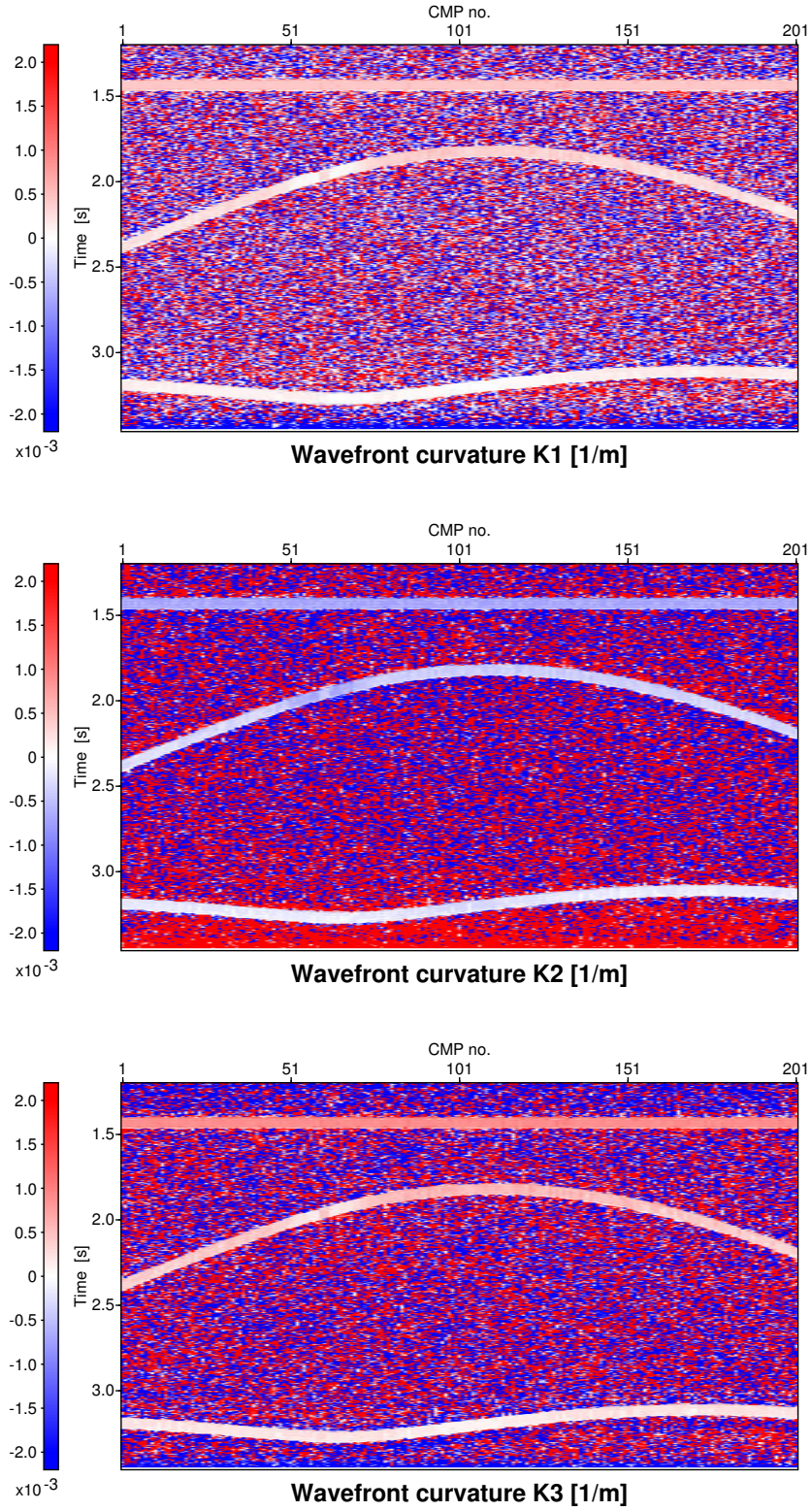

Figure 8: Wavefront curvatures K_1, K_2, and K_3 determined by the CO CRS stack.

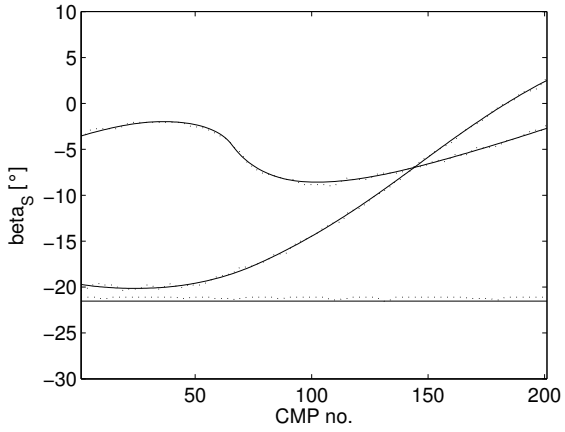

(a) Emergence angle β_S

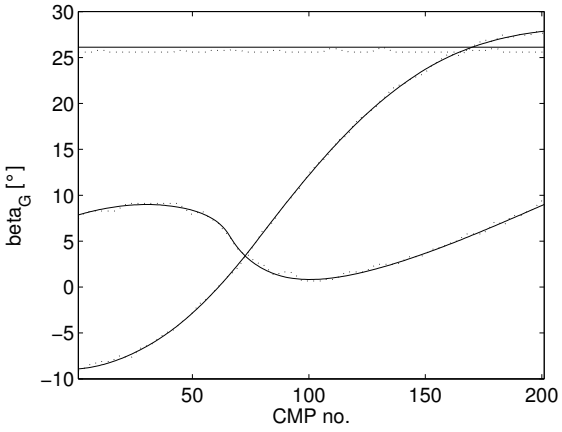

(b) Emergence angle β_G

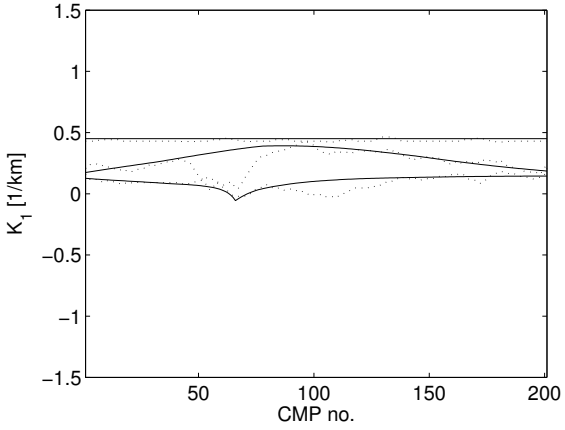

(c) Wavefront curvature K_1

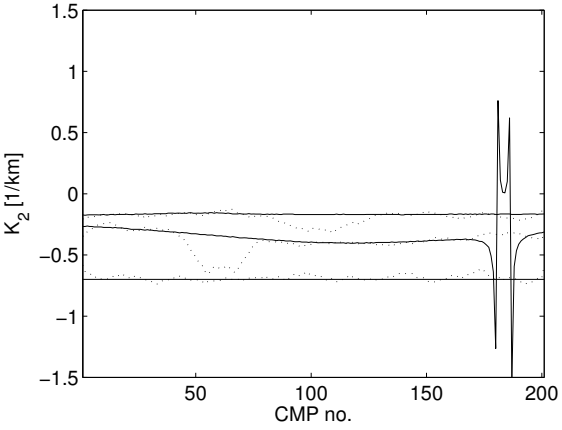

(d) Wavefront curvature K_2

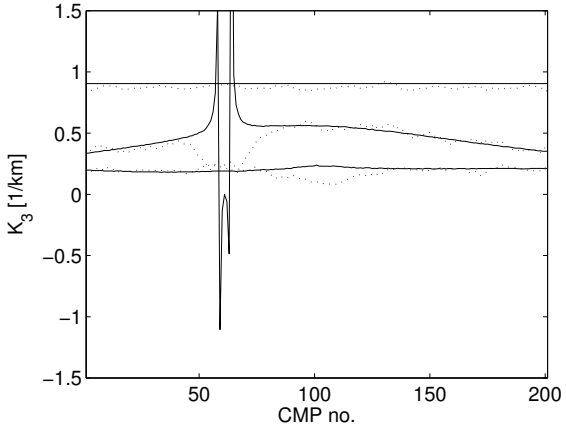

(e) Wavefront curvature K_3

Figure 9: Comparison of model-derived (solid) and data-derived (dotted) wavefield attributes.